Radiation Physics and Chemistry 144 (2018) 125–131

Contents lists available at ScienceDirect

Radiation Physics and Chemistry

journal homepage: www.elsevier.com/locate/radphyschem

Effect of Ar^{9+} irradiation on Zr-1Nb-1Sn-0.1Fe alloy characterized by Grazing Incidence X-ray diffraction technique

Argha Dutta, Kalipada Das, N. Gayathri*, Ranjini Menon, P.Y. Nabhiraj, Paramita Mukherjee

Variable Energy Cyclotron Centre, HBNI, 1/AF Bidhannagar, Kolkata 700064, India

A B S T R A C T

The microstructural parameters such as domain size and microstrain have been estimated from Grazing Incidence X-ray Diffraction (GIXRD) data for Ar^{9+} irradiated Zr-1Nb-1Sn-0.1Fe sample as a function of dpa (dose). Detail studies using X-ray Diffraction Line Profile Analysis (XRDLPA) from GIXRD data has been carried out to characterize the microstructural parameters like domain size and microstrain. The reorientation of the grains due to effect of irradiation at high dpa (dose) has been qualitatively assessed by the texture parameter P (*hkl*).

1. Introduction

Zirconium-based alloys Zircaloy-2 (Zr-2) and Zircaloy-4 (Zr-4) are widely used in nuclear industry as cladding materials for BWRs and PWRs, respectively. Over more than 60 years, these materials displayed a very good combination of properties such as low neutron absorption, creep resistance, resistant to stress-corrosion cracking, reduced hydrogen uptake, resistant to corrosion and/or oxidation especially in the case of Zr-4 (Whitmarsh, 1962; Sabol, 2004; Murty and Charit, 2006; Douglas, 1971). The alloy Zr-1%Nb-1%Sn-0.1Fe has been optimized to have better properties with respect to corrosion resistance, irradiation growth resistance and creep resistance compared to Zr-4 (Nikulina et al., 1996). During the typical life time of the thermal reactor operation, these fuel cladding materials are subjected to a maximum dose of about 10–20 dpa (Idrees et al., 2013). Among the various properties that are affected by irradiation, the most important for Zr based alloys is the irradiation enhanced growth which can lead to different dimensional changes depending upon the microstructure of the unirradiated material. Zr and its alloys have an inherent anisotropy due to its HCP crystal structure (Murty and Charit, 2006). Murty and Charit (2006) have pointed out that the grains are oriented along certain crystallographic direction resulting in the preferred orientation during the processing stage. Hence during the fabrication process, the alignment of the grains can be manipulated in such a way that the changes in the properties due to irradiation can be controlled to a major extent during the life time of the components in the reactor. The initial texture of the fuel tube controls the hydride precipitation and also irradiation induced growth of zirconium-base alloys (Murty and Charit, 2006). The effect of parameters such as temperature, texture, dose and pre-irradiation thermo-mechanical history on the extent of growth has been investigated experimentally by various authors (Kreyns et al., 1966; Hesketh et al., 1969; Ibrahim and Winegar, 1972; Adamson, 1977; Murgatroyd and Rogerson, 1978a, b; Faulkner and MacElroy, 1978). Attempts were also made to correlate the measured growth with the crystallographic texture (Faulkner and MacElroy, 1978; Carpenter and Northwood, 1975; Northwood et al., 1976). However, there is no literature available which shows whether the crystallographic texture changes as a function of dose in the irradiated Zr based alloys particularly at high dpa. Recently, Kurpaska et al. (2016), have reported the effect of 150 KeV Ar-irradiation on pure zirconium coupons at room temperature with fluences ranging from 1×10^{15} to 1×10^{17} cm^{-2}. The result reported does not reveal any conclusive changes with respect to the microstructure.

In this paper, an attempt has been made to qualitatively determine the effect of irradiation by ion beam on the microstructure and texture of the Zr-1Sn-1Nb-0.1Fe alloy using X-ray diffraction technique as a function of dose. The irradiation has been done using Electron Cyclotron Resonance (ECR) ion source by low energy charged particle. ECR provides the charged particles having energy of the order of keV and of high flux. As a result a very high dpa ranging from 10 to 200 dpa could be attained in these samples in a short time and with no radiation hazards. As the damage region is highly localised due to irradiation at low energy (within a region of 200–300 nm), the region has been assessed by Grazing incidence XRD technique as a function of dose. The microstructural parameters have been characterized by X-ray diffraction Line profile analysis (XRDLPA) using different techniques like Williamson-Hall (W-H) plot (Williamson and Hall, 1953), Modified Rietveld Technique (Young, 1993; Lutterotti and Scardi, 1990) and

* Corresponding author.
E-mail address: gayathri@vecc.gov.in (N. Gayathri).

https://doi.org/10.1016/j.radphyschem.2017.11.016
Received 25 January 2017; Received in revised form 21 November 2017; Accepted 26 November 2017
Available online 02 December 2017
0969-806X/

Double Voigt analysis (Balzar and Ledbetter, 1993). The texture parameter P(*hkl*) has also been assessed as a function of dose. The grazing incidence angles were chosen in such a way that it covers the entire damage region and can evaluate the damage as a function of depth. Extensive studies have been carried out on Zirconium based alloys using both light ion and heavy ion at room temperature and high temperature and at various levels of dose and dose rate (Idrees et al., 2013; Mukherjee et al., 2005, 1999; Sarkar et al., 2008; Chowdhury et al., 2011; Neogy et al., 2015). In all these studies, the irradiation was done either by proton or heavy ions of energy in the range of MeV order which makes the bulk penetration possible but the dpa was restricted to 3–4 dpa (peak dpa). Therefore, it is interesting to study the effect at high dpa on the microstructure and the texture of the material.

2. Experimental details

Zr-1Nb-1Sn-0.1Fe samples of 10 mm × 10 mm were mechanically polished before irradiation. The samples were irradiated using Ar^{9+} ion from the ECR ion source at VECC, Kolkata. The energy of the ion was ~ 306 KeV. The range of Ar^{9+} ions in Zr-1Nb-1Sn-0.1Fe samples, and the damage profile were calculated using SRIM 2000 (Ziegler, 2015) and shown in Fig. 1. Maximum depth of penetration of the Ar^{9+} ions was estimated to be ~ 400 nm. The total target displacements of the collision events are shown in Fig. 1. The samples were irradiated to the doses of 1×10^{16} Ar^{9+}/cm^2, 2×10^{16} Ar^{9+}/cm^2, 3×10^{16} Ar^{9+}/cm^2, 4×10^{16} Ar^{9+}/cm^2 and 6×10^{16} Ar^{9+}/cm^2. Damage level has been calculated in terms of displacement per atom (dpa) using the following formula.

$$dpa = \frac{\varphi \times 10^8 \times Damage - rate}{N} \quad (1)$$

where φ is the fluence in ions/cm^2, the damage - rate is in vacancies/(ion) obtained from SRIM, and N is the atomic density in atoms/cm^3. The maximum damage occurred during Ar^{9+} ion irradiation in Zr-1% Nb-1%Sn-0.1Fe is around 200 dpa.

In order to confine the characterization to only in the irradiated region of the sample (~ 400 nm), grazing incidence X-ray diffraction (GIXRD) study using Cu-K_α radiation was performed on the irradiated samples. Irradiations carried out by heavy ions having energy in the range of 100–500 KeV have limited characterization tools essentially because of the fact that the damage is mainly restricted near to the surface (~ 300 nm) which makes the characterization extremely difficult. Grazing Incident X-ray Diffraction Line Profile Analysis(GIXRD-LPA) has been used to study the micro-strain and partitioning of the grains into regions separated by small angle grain boundaries within small volumes of 10^{-3} mm^3 of the irradiated samples (Neogy et al., 2015). In order to access the damage as a function of the depth, the

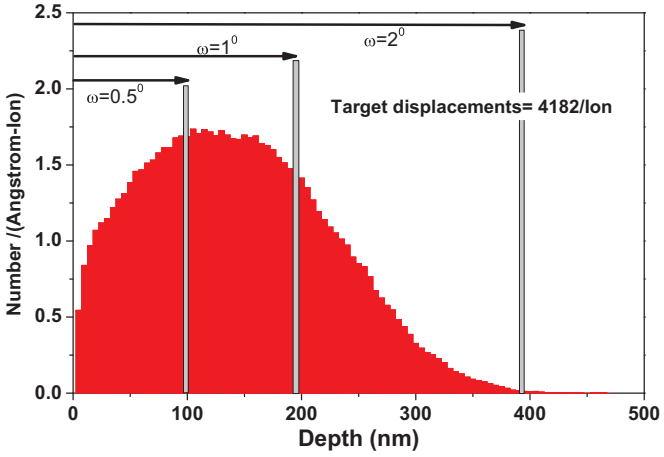

Fig. 1. The range of Ar ions and damage profile in Zirconium using the code SRIM 2000.

GIXRD measurements were performed at three different incident angles (ω) namely 0.5°, 1° and 2°. Different grazing incident angles were used to study the damage region along the thickness direction. The linear absorption coefficient (μ) of Zr is 890.6 cm^{-1} for CuK_α radiation. The depth of penetration (t) of X-ray during GIXRD measurements were calculated using the following relationship at incident angles (ω) 0.5°, 1°, 2° (Thin film analysis, 2005)

$$t = \frac{\sin\omega}{\mu} \quad (2)$$

Using Eq. (2), the depth of penetration of CuK_α is about 980 Å, 1960 Å and 3920 Å respectively at the three different grazing angles used and is marked by the vertical bars and horizontal arrows in Fig. 1. The instrumental broadening (for the parallel beam geometry) is also dependent on the penetration of X-rays within the sample. Therefore, the correction for instrumental broadening was performed at all the three grazing angles using a standard defect free LaB_6 powder.

3. Methods of analysis and discussion

X-ray line profile analysis is an effective and non-destructive technique to characterize the microstructure of the deformed alloys (Warren and Averbach, 1950). The method which is used to separate the strain- and domain-size components of the broadening is originally given by Warren and Averbach (1950). The values obtained by the method are an average (surface-weighted) crystallite size which is related to the crystallite size distribution and an average strain (within a characteristic size), along a particular crystallographic direction (Warren and Averbach, 1950). Wilkens (1970a), Wilkens (1970b) and Wilkens et al. (1980) developed the theory for symmetrical X-ray diffraction lines broadened by dislocation, which was successfully verified by the experimental study of tensile deformed Cu- single crystals (Ungar et al., 1982). There are other techniques like single peak analysis by integral Breadth Method (de Keijser et al., 1982), Williamson Hall technique (Williamson and Hall, 1953), double Voigt method (Balzar and Ledbetter, 1993) and whole powder pattern fitting by Modified Rietveld Technique (Young, 1993; Lutterotti and Scardi, 1990). We have carried out the Line Profile Analysis (LPA) of the GIXRD data using the W-H technique, double Voigt method and whole powder pattern fitting by Modified Rietveld techniques as a function of dose of irradiation as well as with depth of irradiation.

The microstructure of irradiated Zr and Zr-alloy have been characterized mostly by transmission electron microscopy (TEM) (Griffiths, 1988; Fei Long, 2015, Adamson et al, 1974). In most of the cases where the dislocations have the same Burgers vector, the conversion to dislocation density is achieved by the use of appropriate calibration factors, determined by direct measurements of dislocation densities using TEM (Griffiths, 1988; Fei Long, 2015, Adamson et al, 1974). This method in itself is subject to a large degree of experimental error, primarily because the dislocation structures are complex (mixed screw and edge character) and are also not uniformly distributed throughout a given material (Zubicza, 2014). Moreover, the sample preparation for TEM is highly time consuming and may cause some changes in the defect structure during sectioning and polishing (Zubicza, 2014; Mukherjee et al., 2004). On the contrary, the XRDLPA evaluates the microstructural parameters in a statistical manner (Mukherjee et al., 2004; Cullity and Stock, 2001). The analysis is easier, reliable and quick and the specimen preparation requires very little time (Cullity and Stock, 2001).

3.1. Williamson- Hall Technique (W-H technique)

Williamson and Hall (1953) assumed that both size and strain broadened profiles are Lorentzian. It relies on the principle (Williamson and Hall, 1953; Scherrer, 1918) that the approximate formulae for size broadening, β_L, and strain broadening, β_e, vary quite differently with

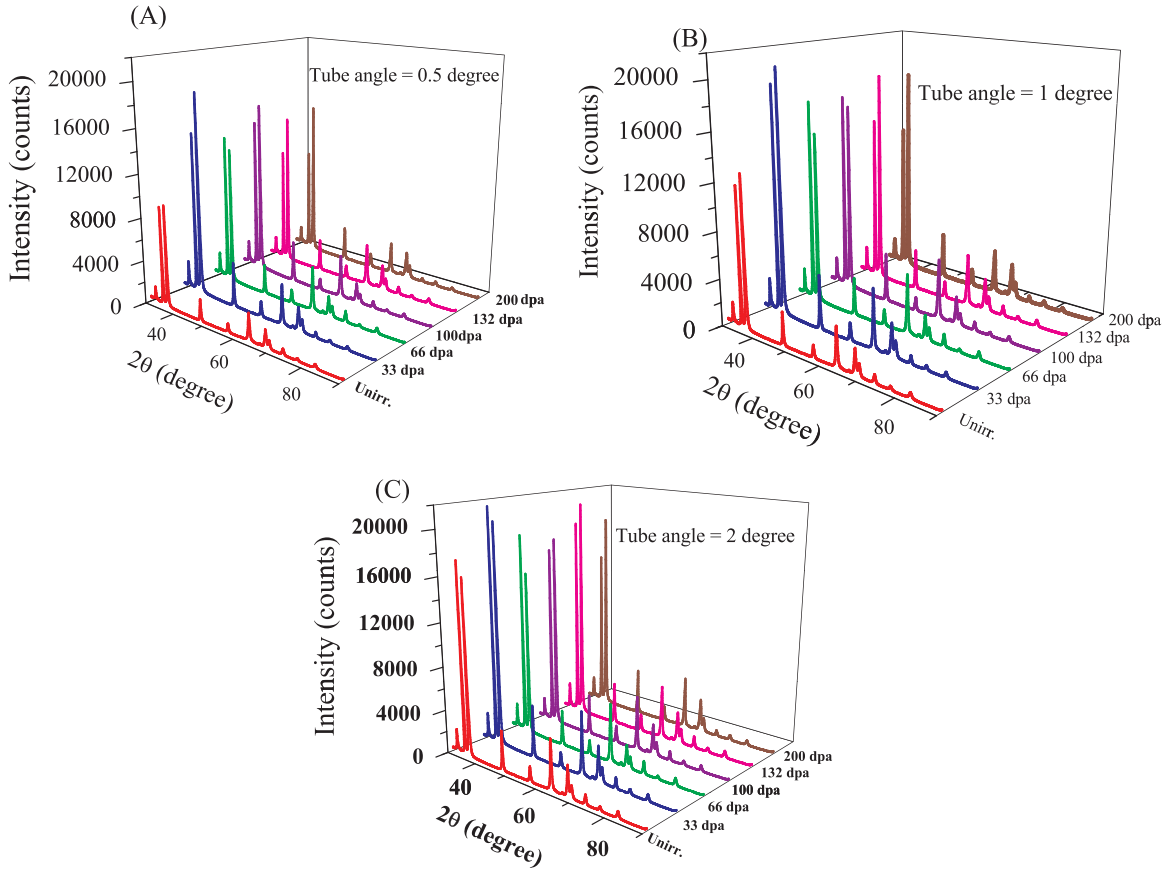

Fig. 2. The room temperature grazing incidence X-ray diffraction patterns of all Zirlo samples of different irradiation doses for incident angles (a) 0.5°, (b) 1° and (c) 2°.

respect to Bragg angle, θ as

$$\beta_L = \frac{K\lambda}{Lcos\theta} \quad \beta_e = C\varepsilon \tan\theta$$

If both the contributions are present simultaneously, their combined effects are generally convoluted. The simplification of Williamson and Hall technique (Williamson and Hall, 1953) is to assume the convolution is a simple sum. So, the expression can be written as,

$$\frac{\beta \cos\theta}{\lambda} = \frac{1}{D_v} + 2\varepsilon\left(\frac{2\sin\theta}{\lambda}\right) \tag{3}$$

The plot of $\left(\frac{\beta\cos\theta}{\lambda}\right)$ versus $S = \left(\frac{2\sin\theta}{\lambda}\right)$ gives the value of microstrain from the slope and volume weighted average domain size from the ordinate intercept (Williamson and Hall, 1953).

3.2. Double Voigt technique

Balzar and Ledbetter (1993) defined the total physically broadened profile as a Voigt function which is basically a convolution of Gaussian and Cauchy function. The Fourier coefficients $F(L)$ in terms of a the undistorted length L, perpendicular to the diffracting planes is obtained by Fourier transform (Balzar and Ledbetter, 1993) and can be written as

$$F(L) = \exp(-2L\beta_C - \pi L^2\beta_G^2) \tag{4}$$

where, β_C and β_G are respectively the Cauchy and Gauss components of total integral breadth β.

β_C and β_G can be written as:

$$\beta_C = \beta_{SC} + \beta_{DC} \tag{5}$$

$$\beta_G^2 = \beta_{SG}^2 + \beta_{DG}^2 \tag{6}$$

where, β_{SC} and β_{DC} are the Cauchy components of size and strain integral breadth respectively and β_{SG} and β_{DG} are the corresponding Gaussian components (Balzar and Ledbetter, 1993).

The size and distortion coefficients are obtained considering at least two reflections from the same family of crystallographic planes (Balzar and Ledbetter, 1993). The surface weighted average domain size D_S and strain $\langle\varepsilon_L^2\rangle^{\frac{1}{2}}$ are given by the equations (Balzar and Ledbetter, 1993):

$$D_S = 1/2\beta_{SC} \tag{7}$$

$$\langle\varepsilon_L^2\rangle = [\beta_{DG}^2/(2\pi) + \beta_{DC}/(\pi^2 L)]/S^2 \text{ where } S = \frac{2\sin\theta}{\lambda} \tag{8}$$

The volume weighted domain size (Scherrer, 1918) is given by: $D_V = \frac{1}{\beta_S}$ where $\beta_S = \frac{\beta\cos\theta}{\lambda}$, integral breadth in the units of S, $(Å)^{-1}$.

The volume weighted column-length distribution functions (Balzar and Ledbetter, 1993) are given by:

$$P_v(L) \propto L\frac{d^2A_S(L)}{dL^2} \tag{9}$$

For a size-broadened profile, the size coefficient is given as:

$$A_S(L) = \exp(-2L\beta_{SC} - \pi L^2\beta_{SG}^2) \tag{10}$$

From Eq. (8), we get,

$$\frac{d^2A_S(L)}{dL^2} = [(2\pi L\beta_{SG}^2 + 2\beta_{SC})^2 - 2\pi\beta_{SG}^2]A_S(L) \tag{11}$$

Selivanov and Smislov (1991) showed that Eq. (11) is a satisfactory approximation of size distribution functions.

3.3. Modified Rietveld method

Modified Rietveld method has been carried out on the diffraction data using the program package MAUD (Lutterotti et al., 1997) using similar procedure described by Wenk et al. (2003). The lattice parameters, the microstructural parameters like the surface weighted coherent domain size (D_S) and r.m.s. microstrain ($\langle\varepsilon_L^2\rangle^{1/2}$) (isotropic) are refined simultaneously using non linear least square fitting taking into account the instrumental broadening and the background parameters. XRD profiles Since, Zirconium based alloys are inherently anisotropic, a strong crystallographic texture is observed along certain crystallographic directions like (002), (101), (103) etc. As a result, the correction for preferred orientation is done by using the spherical harmonics model (Lutterotti et al., 1997; Wenk et al., 2003) for obtaining the best fit. Using this software, the whole XRD pattern is fitted and the values of the best fit are reported for D_S and $\langle\varepsilon_L^2\rangle^{1/2}$.

4. Results

Fig. 1 represents the range of Ar^{9+} ions and damage profile in Zirconium using the code SRIM 2000. Dpa calculation has been done using Eq. (1). The grazing incidence X-ray diffraction (GIXRD) patterns at different doses are shown in Fig. 2. From Fig. 2, it is noted that the intensities of the highest density planes e.g (002), (101) and (103) vary significantly as a function dose of irradiation. Moreover, it is observed that the relative intensities of the peaks (101) and (002) change with the irradiation doses (at all incidence angle of measurements). A detail analysis has been done to evaluate the microstructural parameters like domain size and microstrain within the domain using W-H plot, and Modified Rietveld technique and Double Voigt analysis as mentioned earlier at different depths of irradiation as a function of dose.

Figs. 3a, 3b and 3c represent the W-H plot at different grazing incidence angle (at 0.5°, 1° and 2°) as a function of dose. Table 1 indicates the value of average volume weighted domain size (coherent region) and microstrain obtained from W-H plot with dose of irradiation and also with depth of irradiation. It is clearly seen from Table 1 that the volume weighted domain size and the microstrain did not change considerably even up to the highest dose of irradiation. These changes are also not significant with changing in the grazing incidence angles (as observed from Table 1) which provide the information as a function of depth. We have also carried out GI-XRDLPA using MAUD (Lutterotti et al., 1997) which is a program based on Rietveld refinement. Fig. 4 shows a typical representative fitting of the X-ray diffraction data (at different incidence angles) by MAUD for 132 dpa (dose 4×10^{16} Ar^{9+}/cm^2) sample. The average surface weighted domain size and microstrain are listed in Table 2 at different grazing incidence angle. From Table 2, it is clearly indicated that average size of the surface weighted domain (D_s) did not vary significantly with respect to the unirradiated one. Figs. 5a, 5b and 5c show the average volume weighted domain size and microstrain obtained from Double Voigt technique at different grazing angle of incidence. Here also, it is clearly observed that the volume weighted domain size (D_v) and microstrain did not vary with dose as well as along the depth of penetration. The volume weighted column-length distribution function Pv(L) along < 00l > normal to the diffraction plane has been shown in Fig. 6. It is evident from Fig. 6 that the column length distribution is comparable for the irradiated samples

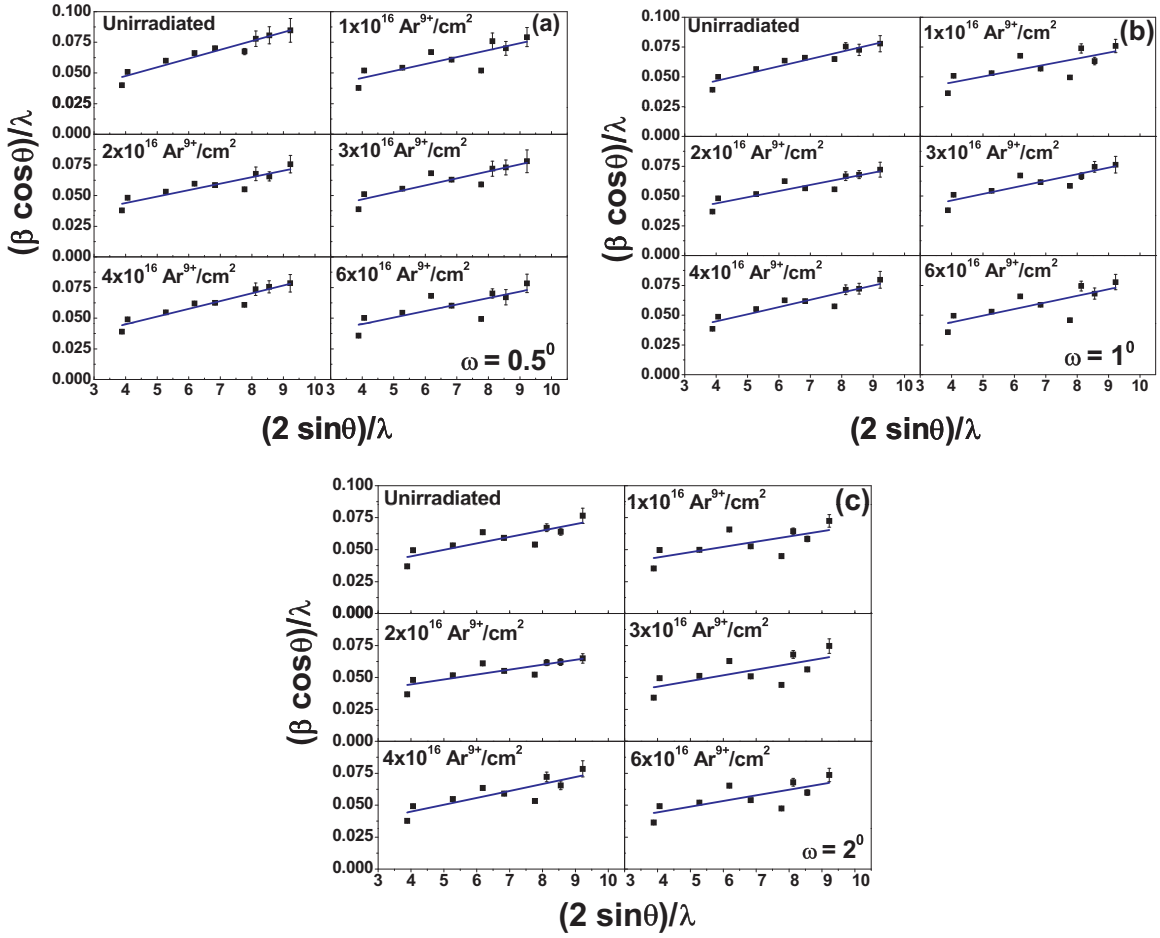

Fig. 3. Williamson Hall plot obtained from GIXRD data for the unirradiated and all irradiated samples at tube angle a) 0.5°, b) 1° & c) 2°.

Table 1
The average volume weighted domain size and microstrain values obtained from the Williamson-Hall plot for unirradiated and all irradiated samples at tube angle 0.5, 1 & 2°.

Tube angle (ω)	Dose (Ar^{9+}/cm^2)	Dose (dpa)	Domain size (D_V) (nm) Error: ± 15%	Microstrain (ε) Error: ± 15%
0.5°	0	0	47	0.004
	1×10^{16}	33	39	0.003
	2×10^{16}	66	39	0.003
	3×10^{16}	100	37	0.003
	4×10^{16}	132	46	0.003
	6×10^{16}	200	38	0.003
1°	0	0	41	0.003
	1×10^{16}	33	36	0.003
	2×10^{16}	66	39	0.003
	3×10^{16}	100	37	0.003
	4×10^{16}	132	44	0.003
	6×10^{16}	200	41	0.003
2°	0	0	37	0.003
	1×10^{16}	33	33	0.002
	2×10^{16}	66	31	0.002
	3×10^{16}	100	36	0.002
	4×10^{16}	132	39	0.003
	6×10^{16}	200	34	0.002

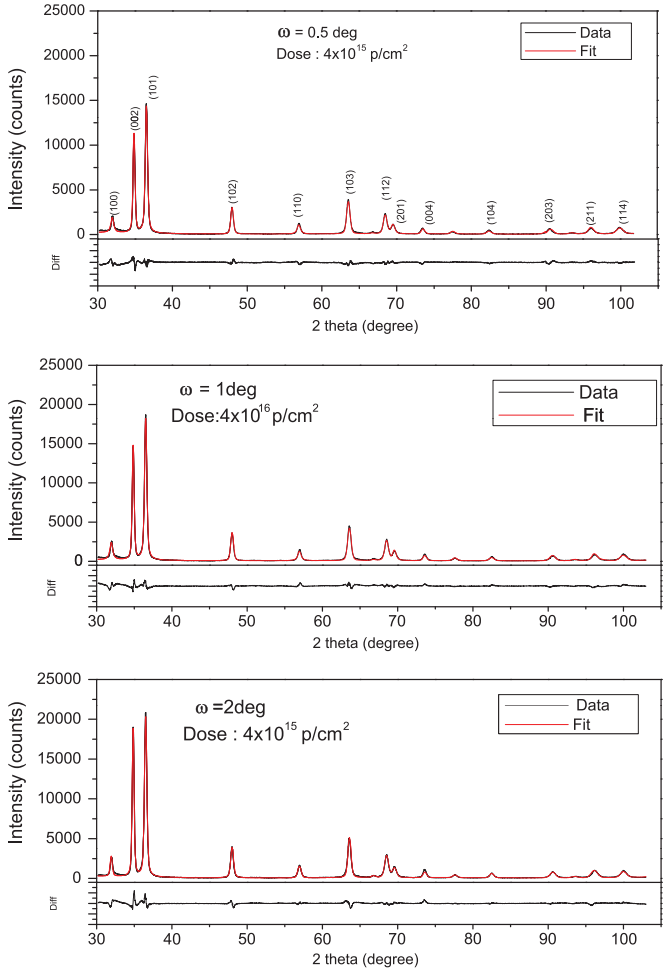

Fig. 4. X-ray diffraction data for the three different incidence angles fitted by MAUD.

with the unirradiated one. The dose of irradiation did not have much effect on the size distribution of the domains. However, these results are contradicted with our earlier studies on proton and heavy ion irradiated zirconium base alloys (Mukherjee et al., 2005, 1999; Sarkar et al., 2008; Chowdhury et al., 2011; Neogy et al., 2015) at a much lower dpa, where in all cases, both the surface weighted and volume weighted domain size decreased and microstrain increased with dose of irradiation.

Interestingly, there is a variation of intensity values of high intensity peaks as a function of dose particularly for (002), (101), (102) and (103) which was not observed in our earlier studies (Mukherjee et al., 2005, 1999; Sarkar et al., 2008; Chowdhury et al., 2011; Neogy et al., 2015). The change in the relative intensities due to irradiation has been qualitatively evaluated using Eq. (12) and shown in Fig. 7.

$$P(hkl) = \frac{I(hkl)_{Irradiated}/I(hkl)_{Unirradiated}}{\sum (I(hkl)_{Irradiated}/I(hkl)_{Unirradiated})} \quad (12)$$

Here, $P(hkl)$ has been used as a quantity which will represent the orientation of a particular set of crystallographic planes. Fig. 7 represents the plot of P(*hkl*) for (002), (101), (102) and (103) planes as a function of dose. It is clearly observed that P(*hkl*) has a significant variation with dose. Initially, at 33 dpa, the value of P(*hkl*) lies between 0.09 and 0.10 for all the prominent peaks. With irradiation, P(*hkl*) for (002) decreases drastically at higher doses. On the other hand, P(*hkl*) for (101) initially decreases and then increases. This indicates that the deformation texture developed during fabrication of cladding tubes has become more randomised and may be compared with the recrystallisation texture of Zr alloys (Tenckhoff, 1988, 2005). This may be attributed to the reorientation of grains occurred due to the large amount of energy deposited during irradiation within a localised volume of irradiated material (10^7 μm^3). As a result, at high dpa, the texturing effect became much more pronounced than the creation of incoherent region (domains) due to evolution of defect clusters. Hence, even at a very high dpa, the domain size and microstrain did not change significantly as compared to irradiated sample. In our earlier studies (Mukherjee et al., 2005, 1999; Sarkar et al., 2008; Chowdhury et al., 2011; Neogy et al., 2015), the irradiation effects were not localised, rather the penetration of the charged particles was up to tens of microns to few hundreds of microns depending upon the energy of the particle. Consequently, the formation of point defect clusters, dislocation loops were much more predominant and no variation of texture was observed even up to the highest dose of irradiation.

5. Conclusion

The microstructural parameters such as domain size and microstrain have been estimated from GIXRD data for Ar^{9+} irradiated Zr-1Nb-1Sn-0.1Fe sample as a function of dpa (dose). The variation of intensity with dose has been correlated with texture parameter P(*hkl*) for different crystallographic planes to understand the effect of very high dpa on the orientation of the grains. It is clearly observed that the domain size and microstrain which was expected to change due to the effect of irradiation remained almost invariant with dose. On the contrary, P(*hkl*)

Table 2
The average surface weighted domain size and microstrain values obtained from GIXRD data for the unirradiated & irradiated samples by the Modified Rietveld Technique at tube angles 0.5°, 1° & 2°.

Tube angle (ω)	Dose (Ar^{9+}/cm^2)	Dose (dpa)	Domain size (D_s) (nm) (Error: ± 10%)	Microstrain (ε) (Error: ± 10%)
0.5°	0	0	60	0.002
	1×10^{16}	33	53	0.002
	2×10^{16}	66	51	0.002
	3×10^{16}	100	49	0.002
	4×10^{16}	132	49	0.002
	6×10^{16}	200	47	0.002
1°	0	0	66	0.002
	1×10^{16}	33	59	0.002
	2×10^{16}	66	51	0.002
	3×10^{16}	100	47	0.002
	4×10^{16}	132	47	0.001
	6×10^{16}	200	46	0.001
2°	0	0	78	0.002
	1×10^{16}	33	68	0.002
	2×10^{16}	66	59	0.002
	3×10^{16}	100	62	0.002
	4×10^{16}	132	58	0.002
	6×10^{16}	200	56	0.002

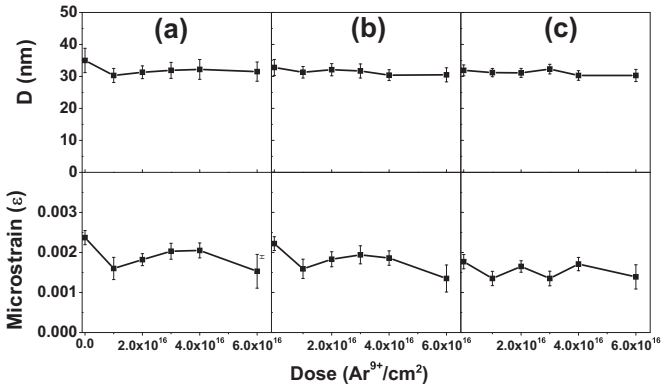

Fig. 5. The variation in the average volume weighted domain size and the microstrain as a function of dose obtained from Double Voigt technique for Grazing Incident angle a) 0.5°, b) 1° and c) 2°.

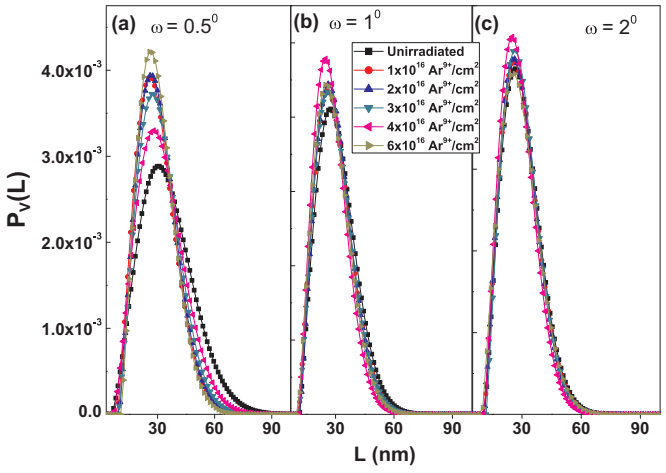

Fig. 6. The volume weighted column length distribution function obtained by Double-Voigt technique for the unirradiated and all irradiated samples at incident angles a) 0.5° b) 1° and c) 2°.

has significantly varied with higher dpa particularly for (101), (002), (102) and (103) planes. This indicates that the energy deposited due to irradiation within a very localised region must have caused reorientation of the grains which has resulted a change in the texture parameter P(*hkl*).

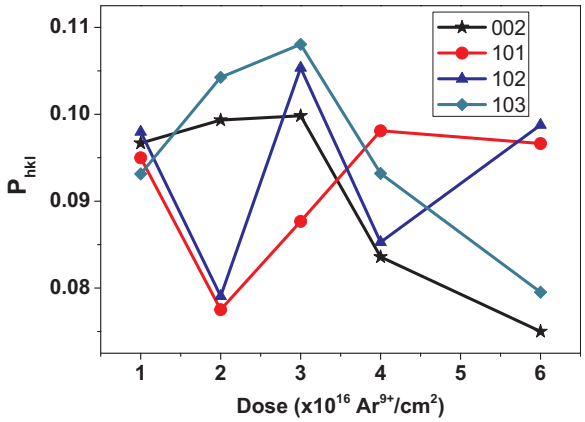

Fig. 7. The change of the crystallographic orientation (P(*hkl*)) due to irradiation as a function of dose. (P(*hkl*) values for major crystallographic planes (002), (101), (102) and (103) are only shown.

References

Adamson, R.B., 1977. Zirconium in the Nuclear Industry. In: ASTM STP 633. ASTM, Philadelphia, pp. 326.

Adamson, R.B., Bell, W.L., Lee, D., 1974. Use of ion bombardment to study Irradiation damage in Zirconium alloys in Zirconium in Nuclear Applications, ASTM STP 551. American Society of Testing of materials 215–228.

Balzar, D., Ledbetter, H., 1993. J. Appl. Cryst. 26, 97–103.

Birkholz, Mario, 2005. Thin Film Analysis by X-ray Scattering. Wiley-VCH Verlag GmbH Co., Weinheim.

Carpenter, G.J.C., Northwood, D.O., 1975. J. Nucl. Mater. 56, 260.

Chowdhury, P.S., Mukherjee, P., Gayathri, N., Bhattacharya, M., Chatterjee, A., Barat, P., 2011. PMG Nambissan. Bull. Mater. Sci. 34, 507–513.

Cullity, B.D., Stock, S.R., 2001. Elements of X-Ray Diffraction, 3rd ed. Pearson.

Douglas, D.L., 1971. The Metallurgy of Zirconium. International Atomic Energy Agency, Vienna.

Faulkner, D., MacElroy, R.J., 1978. In: Proceedings of the 9th Intern. Symp. on Effects of Radiation in Structural Materials, Richland, WA, ASTM.

Fei Long, 2015. Characterization of deformation mechanisms in zirconium alloys: Effect of temperature and irradiation, A thesis submitted to the Department of Mechanical and Materials Engineering In conformity with the requirements for the degree of Doctor of Philosophy Queen's University Kingston, Ontario, Canada (February, 2015).

Griffiths, M., 1988. A review of microstructure evolution in zirconium alloys during irradiation. J. Nucl. Mater. 159, 190–218.

Hesketh, R.V., Harbottle, J.E., Waterman, N.A., Lobb, R.C., 1969. In: Radiation Damage in Reactor Materials, Vol. 1 (IAEA, Vienna), p. 365.

Ibrahim, E.F., Winegar, J.E., 1972. J. Nucl. Mater. 45/73) 335.

Idrees, Y., Yao, Z., Sattari, M., Kirk, M.A., Daymond, M.R., 2013. Irradiation induced microstructural changes in Zr-Excel alloy. J. Nucl. Mater. 441, 138–151.

de Keijser, T.H., Langford, J.I., Mittemeijer, E.J., Vogels, A.B.P., 1982. Use of the Voigt function in a single-line method for the analysis of X-ray diffraction line broadening.

J. Appl. Crystallogr. 15, 308–314.
Kreyns, P.H., Duncombe, quotedbyE., Mayer, E.J., Coffman, W.A., 1966. Westinghouse (US) Report WAPDTM-583 p. 35.
Kurpaskaa, L., et al., Gapinskab, M., Jasinskic, J., Lesniakd, M., Sitarzd, M., Nowakowska-Langiera, K., Jagielskia, J., Wozniak, K., 2016. Influence of Ar-irradiation on structural and nanomechanical properties of pure zirconium measured by means of GIXRD and nanoindentation techniques. J. Mol. Struct. 1126, 226–231.
Lutterotti, L., Scardi, P., 1990. Simultaneous structure and size–strain refinement by the Rietveld method. J. Appl. Crystallogr. 23, 246–252.
Lutterotti, L., Matthies, S., Wenk, H.-R., Schultz, A.S., Richardson Jr., J.W., 1997. J. Appl. Phys. 81, 594.
Mukherjee, P., Sarkar, A., Barat, P., 2005. Microstructural changes in oxygen-irradiated zirconium-based alloy characterised by X-ray diffraction techniques. Mater. Charact. 55, 412–417.
Mukherjee, P., Nambissan, P.M.G., Sen, P., Barat, P., Bandyopadhyay, S.K., 1999. Proton irradiation effects in Zr-1.0 Nb-1.0 Sn-0.1 Fe probed by positron annihilation. J. Nucl. Mater. 273, 338–342.
Mukherjee, P., Sarkar, A., Barat, P., Bandyopadhyay, S.K., Pintu Sen, Chattopadhyay, S.K., Chatterjee, P., Chatterjee, S.K., Mitra, M.K., 2004. Acta Mater. 52, 5687.
Murgatroyd, R.A., Rogerson, A., 1978. UKAEA Report ND-R-204(R).
Murgatroyd, R.A., Rogerson, A., 1978b. In: Proceedings of the 4th Intern. Conference on Zirconium in the Nuclear Industry, Stratford-on-Avon, ASTM.
Murty, K.L., Charit, I., 2006. Texture development and anisotropic deformation of zircaloys. Prog. Nucl. Energy 48, 325–359.
Neogy, S., Mukherjee, P., Srivastava, A.P., Singh, M.N., Gayathri, N., Sinha, A.K., et al., 2015. Proton irradiation of Zr–1wt% Nb cladding material: a depth-wise assessment of inhomogeneous microstructural damage using X-ray diffraction line profile analyses. J. Alloy. Compd. 640, 175–182.
Nikulina, A.V., Markelov, V.A., Peregud, M.M., Voevodin, V.N., Panchenko, V.L., Kobylyansky, G.P., 1996. Irradiation-induced microstructural changes in Zr-1% Sn-1% Nb-0.4% Fe. J. Nucl. Mater. 238, 205–210.
Northwood, D.O., Fidleris, V., Gilbert, R.W., Carpenter, G.J.C., 1976. J. Nucl. Mater. 61, 123.
Sabol, G.P., 2004. in Zirconium in the Nuclear Industry In: Proceedings of the 14th International Symposium, Stockholm, Sweden, ASTM International, STP 1467, p.3.
Sarkar, A., Mukherjee, P., Barat, P., 2008. Effect of heavy ion irradiation on microstructure of zirconium alloy characterised by X-ray diffraction. J. Nucl. Mater. 372, 285–292.
Scherrer, P., 1918. Nachr. Gott 2, 98–100.
Selivanov, V.N., Smislov, E.F., 1991. Zavod Lab 57, 28–29.
Tenckhoff E., 1988. Deformation mechanisms, texture and anisotropy in Zirconium and Zircaloy, ASTM, Special technical publication (STP 966), Philadelphia.
Tenckhoff, E., 2005. Review of deformation mechanisms, texture, and mechanical anisotropy in zirconium and zirconium base alloys. J. ASTM Int. 2 (4), 1–2.
Ungar, T., Mughrabi, H., Wilkens, M., 1982. Acta Metall. 30, 1861–1867.
Warren, B.E., Averbach, B.L., 1950. J. Appl. Phys. 21, 595.
Wenk, H.-R., Lutterotti, L., Vogel, S.C., 2003. Nucl. Instr. Methods A 515, 575.
Whitmarsh, L., 1962. Review of Zircaloy-2 and Zircaloy-4 Properties Relevant to N.S. Savannah Reactor Design, ORNL-3281, Oak Ridge National Laboratory.
Wilkens, M.1970a. In Fundamental Aspects of Dislocation Theory, edited by J. A. Simmons, R. De. Wit and R. Bollough, vol. II, pp. 1195–1221. Natl. Bur. Stand. (US) Spec. Publ. No. 317. Washington, DC, USA.
Wilkens, M., 1970b. Phys. Status Solidi A 2, 359–370.
Wilkens, M., Herz, K., Mughrabi, H., 1980. Z. Met. 71, 376–384.
Williamson, G.K., Hall, W.H., 1953. X-ray line broadening from filed aluminium and wolfram. Acta Metall. 1, 22–31.
Young, R.A., 1993. The Rietveld Method. Oxford University Press.
Ziegler, J., 2015. SRIM - The Stopping and Range of Ions in Matter, 15th ed. . http://www.srim.org/.
Zubicza, Jeno, 2014. X-ray line profile analysis in Materials Science, IGI Global.